
Generalized Laplace Approximation

Yinsong Chen
School of Engineering
Deakin University
Melbourne, VIC, 3216, Australia
chenyins@deakin.edu.au

Samson S. Yu
School of Engineering
Deakin University
Melbourne, VIC, 3216, Australia
s.yu@ieee.org

Zhong Li
Faculty of Mathematics and Computer Science
FernUniversität in Hagen
Hagen, 58084, Germany
zhong.li@fernuni-hagen.de

Chee Peng Lim
Institute for Intelligent Systems Research and Innovation
Deakin University
Melbourne, VIC, 3216, Australia
chee.lim@deakin.edu.au

Abstract

In recent years, the inconsistency in Bayesian deep learning has garnered increasing attention. Tempered or generalized posterior distributions often offer a direct and effective solution to this issue. However, understanding the underlying causes and evaluating the effectiveness of generalized posteriors remain active areas of research. In this study, we introduce a unified theoretical framework to attribute Bayesian inconsistency to model misspecification and inadequate priors. We interpret the generalization of the posterior with a temperature factor as a correction for misspecified models through adjustments to the joint probability model, and the recalibration of priors by redistributing probability mass on models within the hypothesis space using data samples. Additionally, we highlight a distinctive feature of Laplace approximation, which ensures that the generalized normalizing constant can be treated as invariant, unlike the typical scenario in general Bayesian learning where this constant varies with model parameters post-generalization. Building on this insight, we propose the generalized Laplace approximation, which involves a simple adjustment to the computation of the Hessian matrix of the regularized loss function. This method offers a flexible and scalable framework for obtaining high-quality posterior distributions. We assess the performance and properties of the generalized Laplace approximation on state-of-the-art neural networks and real-world datasets.

1 Introduction

Bayesian inference stands as a pivotal scientific learning framework utilized today. Its fundamental tenet involves employing probability to quantify all forms of uncertainty within a statistical model and subsequently updating this uncertainty in light of observed data using Bayes theorem (Jospin

et al. [2022]),

$$p(\mathcal{H}|\mathcal{D}) = \frac{p(\mathcal{D}|\mathcal{H})p(\mathcal{H})}{p(\mathcal{D})} = \frac{p(\mathcal{D}|\mathcal{H})p(\mathcal{H})}{\int_{\mathcal{H}} p(\mathcal{D}|\mathcal{H}')p(\mathcal{H}')d\mathcal{H}'} \quad (1)$$

Here, \mathcal{H} represents a hypothesis with associated prior belief, while $\mathcal{D} := \{(x_n, y_n)\}_{n=1}^N$ denotes N observed data samples informing one's belief about \mathcal{H} . $p(\mathcal{H})$ represents the prior, $\int_{\mathcal{H}} p(\mathcal{D}|\mathcal{H}')p(\mathcal{H}')d\mathcal{H}'$ is the evidence, and $p(\mathcal{H}|\mathcal{D})$ is referred to as the posterior.

In the past decade, it has become evident that Bayesian inference can exhibit inconsistent behavior when confronted with model misspecification (Grünwald and Langford [2007], Erven et al. [2007], Müller [2013], Holmes and Walker [2017], Grünwald and van Ommen [2017], Yao et al. [2018], Syring and Martin [2019], Grünwald and Mehta [2020]). For instance, Grünwald and van Ommen [2017] demonstrate the inconsistency of Bayesian inference when models are misspecified, exemplified by applying a standard linear model assuming homoskedasticity to heteroskedastic data without outliers. As sample size increases, the posterior probability is observed to progressively support more complex yet inferior models.

A prevalent solution to address model misspecification involves augmenting Bayesian inference with a learning rate parameter denoted as \mathcal{T} , also referred to as temperature in Gibbs posterior literature.

$$p(\mathcal{H}|\mathcal{D}) = \frac{p(\mathcal{D}|\mathcal{H})^{\mathcal{T}}p(\mathcal{H})}{\int_{\mathcal{H}} p(\mathcal{D}|\mathcal{H}')^{\mathcal{T}}p(\mathcal{H}')d\mathcal{H}'} \quad (2)$$

This method, termed generalized or tempered Bayes, has been proposed independently by multiple authors (Barron and Cover [1991], Walker and Hjort [2001], Zhang [2006], Grünwald [2012], Bissiri et al. [2016]). The role of \mathcal{T} is evident; for $0 < \mathcal{T} < 1$, the impact of the prior is emphasized more than in the standard Bayesian update, resulting in reduced influence from the data. In contrast, for $\mathcal{T} > 1$, the likelihood gains prominence over the standard Bayesian update, and in extreme cases with very large \mathcal{T} , the posterior concentrates on the maximum likelihood estimator for the model. In the extreme case when $\mathcal{T} = 0$, the posterior consistently equals the prior. In statistical Bayesian inference, \mathcal{T} is typically selected to be less than one (Heide et al. [2020]).

A comparable challenge and resolution have been identified in the realm of Bayesian deep learning (Guo et al. [2017], Wenzel et al. [2020], Osawa et al. [2019]). In this study, we differentiate Bayesian deep learning from conventional statistical Bayesian inference. While they share the same theoretical foundation, Bayesian deep learning typically operates with larger datasets and more complex data structures, necessitating scalable learning methodologies such as the Hamiltonian Monte Carlo algorithm (Neal et al. [2011]), variational inference (Blei et al. [2017]), Laplace approximation (Daxberger et al. [2021]), and sophisticated models like deep neural networks. In contrast to identifying model misspecification as the cause of inconsistency in Bayesian inference, (Wenzel et al. [2020]) pinpoint the poor quality of the prior as a potential contributor to inconsistent behavior in Bayesian deep learning. Furthermore, as documented in the Bayesian deep learning literature (Zhang et al. [2018], Leimkuhler et al. [2019], Heek and Kalchbrenner [2019], Zhang et al. [2020]), \mathcal{T} is commonly chosen to exceed one. It is noteworthy that the model parameters, denoted as θ , are typically used to represent the hypothesis \mathcal{H} in Bayesian deep learning. Moreover, in certain studies such as (Wenzel et al. [2020]), a tempered or generalized posterior of this nature can also arise

$$p(\theta|\mathcal{D}) = \frac{p(\mathcal{D}|\theta)^{\mathcal{T}}p(\theta)^{\mathcal{T}}}{\int_{\theta} p(\mathcal{D}|\theta')^{\mathcal{T}}p(\theta')^{\mathcal{T}}d\theta'} \quad (3)$$

Assuming Gaussian priors over the model parameters, i.e., $p(\theta) = \mathcal{N}(0, \sigma)$, as is often the case in Bayesian neural networks, Eq. (3) is essentially Eq. (2) with rescaled prior variances (Aitchison [2020]). The derivation is straightforward:

$$\begin{aligned} \frac{1}{\mathcal{T}} \log p(\theta) &= -\frac{1}{2\mathcal{T}\sigma^2} \sum_{n=1}^N \theta_n^2 + \text{const.} = -\frac{1}{2(\sqrt{\mathcal{T}}\sigma)^2} \sum_{n=1}^N \theta_n^2 + \text{const.} = \log p'(\theta), \\ p'(\theta) &= \mathcal{N}(0, \sqrt{\mathcal{T}}\sigma). \end{aligned} \quad (4)$$

Our primary contributions are twofold: 1) a unified theoretical framework for interpreting how the generalized posterior addresses model misspecification in statistical Bayesian learning and

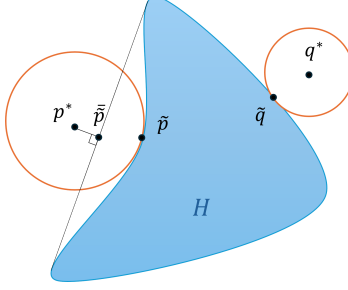


Figure 1: Model misspecification.

inadequate priors in Bayesian deep learning (Section 2), and 2) a generalized Laplace approximation method that incorporates the concept of generalized Bayes into Laplace approximation (Section 3). Our experimental results (Section 4) demonstrate that the generalized Laplace approximation can enhance performance on in-distribution data with an appropriately chosen \mathcal{T} , though the optimal \mathcal{T} is significantly influenced by the selected Hessian approximation. Additionally, we show the susceptibility of the generalized Laplace approximation to out-of-distribution data caused by domain shift.

2 How Generalized Bayes Can Resolve Model Misspecification and Poor Prior

In this section, we first review the theory of how generalized Bayes can address model misspecification in statistical Bayesian inference. We then extend this concept to Bayesian deep learning, explaining how generalized Bayes can resolve both model misspecification and poor prior issues.

2.1 How Generalized Bayes Can Resolve Model Misspecification

To gain a clearer understanding of model misspecification, let us commence with an intuitive example initially presented in (Grünwald and van Ommen [2017]). As depicted in Fig. 1, when the 'ground truth' p^* lies beyond the hypothesis space \mathcal{H} , indicating model misspecification, and the model is non-convex, the distribution $\tilde{p}(y|x)$ minimizing the Kullback-Leibler (KL) divergence to the 'ground truth' p^* within the convex hull of \mathcal{H} can significantly differ from \tilde{p} . Here, \tilde{p} denotes the distribution in the hypothesis space that minimizes KL divergence to the 'true' p^* . In cases where q^* rather than p^* represents the true distribution, the convexity property enables \tilde{q} to attain the minimum. Therefore, one trivial explanation for why Bayesian deep learning does not experience issues with model misspecification could be that, in cases of overparameterization, the optimization landscape of neural networks is nearly convex (Du et al. [2018], Li and Liang [2018], Allen-Zhu et al. [2019]).

Grünwald and van Ommen [2017] offer an explanation for the efficacy of the \mathcal{T} -generalized posterior in correcting Bayesian updates when models are misspecified: for sufficiently small \mathcal{T} , it is formally identical to a conventional posterior derived from an adjusted joint probability model. To delve into this interpretation, we start with specific settings. A learning problem is defined by a tuple $(l, \mathcal{P}, \mathcal{F})$ (Vapnik [2013]), where \mathcal{P} represents distributions over a sample space $\mathcal{Z} := \mathcal{X} \times \mathcal{Y}$, \mathcal{F} denotes a set of models (also known as the hypothesis space \mathcal{H} in certain Bayesian literature), and $l := \mathcal{F} \times \mathcal{Z} \rightarrow \mathbb{R} \cup \{\infty\}$ denotes a loss function.

Let $h^*(x, y)$ denote the density function of the true distribution p^* on $Z := (X, Y) \in \mathcal{P}$. The \mathcal{T} -generalized distributions $p^{(\mathcal{T})}$ are formally defined as joint distributions over Z with density functions $h^{(\mathcal{T})}$:

$$h^{(\mathcal{T})}(x, y|\theta) = h^*(x, y) \left(\frac{h(y|x, \theta)}{h(y|x, \tilde{\theta})} \right)^{\mathcal{T}}, \quad (5)$$

extended to sample size by independence, where $\tilde{\theta}$ minimizes the loss function, typically represented by the negative log-likelihood (NLL) in our context. To derive the interpretation, we introduce an auxiliary definition.

Definition 1 (Central Condition ((Grünwald and Mehta [2020]))) For $\mathcal{T} > 0$, $(l, \mathcal{P}, \mathcal{F})$ satisfies the \mathcal{T} -strong central condition if there exists a $\tilde{f} \in \mathcal{F}$ such that

$$E[e^{\mathcal{T}(l(\tilde{f}, Z) - l(f, Z))}] \leq 1, \text{ for all } f \in \mathcal{F} \text{ and } Z \in \mathcal{P}. \quad (6)$$

Lemma 1 In a learning problem adhering to the $\tilde{\mathcal{T}}$ -strong central condition, selecting any $0 < \mathcal{T} \leq \tilde{\mathcal{T}}$ results in the following:

$$\int \int h^{(\mathcal{T})}(x, y|\theta) dx dy \leq 1, \text{ for any } \theta \text{ in hypothesis space}. \quad (7)$$

Proof of Lemma 1. Substituting l with NLL function and \mathcal{T} with $\tilde{\mathcal{T}}$ into Eq. (6), we obtain

$$E_{(x,y) \sim (X,Y)}[e^{\tilde{\mathcal{T}}(-\log(h(y|x, \tilde{\theta})) + \log(h(y|x, \theta)))}] = E_{(x,y) \sim (X,Y)}[(\frac{h(y|x, \theta)}{h(y|x, \tilde{\theta})})^{\tilde{\mathcal{T}}}] \leq 1. \quad (8)$$

Based on the condition $\int \int h^*(x, y) dx dy = 1$, Eq. (7) can be readily derived.

When Eq. (7) equals 1, the model is considered correctly specified, rendering the use of \mathcal{T} unnecessary. If Eq. (7) is strictly less than 1, denoted as $1 - \epsilon$, then the corresponding $p^{(\mathcal{T})}$ can be interpreted as a standard probability distribution. This interpretation involves defining it on an extended outcome space $(\mathcal{X} \times \mathcal{Y}) \cup \{\square\}$ and assuming that it assigns probability mass ϵ to a pseudo outcome \square , which in reality would not occur. Thus, the \mathcal{T} -generalized Bayes can be understood as updating the posterior using the likelihood derived from a correctly specified probability model.

Having elucidated the reasons behind Bayesian inconsistency due to model misspecification and how it is addressed through the \mathcal{T} -generalized posterior in the context of statistical Bayesian inference, another aspect requiring resolution is the determination of when the central condition holds. Notably, the strong central condition is trivially fulfilled for density estimation when the model is accurately specified. Additionally, it automatically holds under a convex model in cases of model misspecification (Van Erven et al. [2015]). Furthermore, for classification and other cases involving bounded excess loss, it can be linked to the Bernstein condition (Bartlett et al. [2005]).

2.2 A Unified Framework for Explaining How Generalized Bayes Can Resolve Model Misspecification and Poor Prior

After the exposition and clarification of the operation of the \mathcal{T} -generalized posterior in statistical Bayesian inference, can we extend the theory to apply it to Bayesian deep learning, thereby bridging the gap? In this scenario, we assume that the temperature factor \mathcal{T} in Bayesian deep learning not only corrects the model but also adjusts the prior based on aforementioned discussion. Let $g(\theta)$ represent the density function of the prior distribution $p(\theta)$.

$$\begin{aligned} p(\mathcal{D}|\theta)^{\mathcal{T}} p(\theta) &= \int \int h^{(\mathcal{T})}(x, y|\theta) g(\theta) dx dy \\ &= \int \int h^{(t)}(x, y|\theta) \left(\frac{h(y|x, \theta)}{h(y|x, \tilde{\theta})}\right)^{(\mathcal{T}-t)} g(\theta) dx dy \\ &= \int \int h^{(t)}(x, y|\theta) g^{(\mathcal{T}-t)}(\theta) dx dy, \end{aligned} \quad (9)$$

where $\mathcal{T} \geq t > 0$ and

$$g^{(\mathcal{T}-t)}(\theta) = g(\theta) \left(\frac{h(y|x, \theta)}{h(y|x, \tilde{\theta})}\right)^{(\mathcal{T}-t)}. \quad (10)$$

Moreover, the subsequent fact can be trivially deduced from the definition of the central condition.

Fact 1: Given $\mathcal{T} > 0$, let $(l, \mathcal{P}, \mathcal{F})$ denote an arbitrary learning problem that fulfills the \mathcal{T} -strong central condition. Then, for any $0 < \mathcal{T}' \leq \mathcal{T}$ and for any $\mathcal{P}' \subseteq \mathcal{P}$, $(l, \mathcal{P}', \mathcal{F})$ also meets the \mathcal{T}' -strong central condition.

By employing the transformation outlined in Eq. (9), we can derive a t -reweighed likelihood distribution and a $(\mathcal{T} - t)$ -reweighed prior distribution. Referring to **Fact 1**, we can conclude that

if the learning problem adheres to the \mathcal{T} -strong central condition, it also meets the t -strong central condition and $(\mathcal{T} - t)$ -strong central condition. Additionally, the \mathcal{T} -strong central condition is inherently satisfied under the convexity ensured by overparameterized neural networks, as discussed in (Van Erven et al. [2015], Grünwald and Mehta [2020]). Therefore, we ensure that $t > 0$ and maintain the t -strong central condition to preserve the aforementioned capability of correcting model misspecification.

Furthermore, Eq. (10) can be interpreted as employing the data samples to adjust the prior. By demonstrating $E_{(x,y) \sim (X,Y)}[(\frac{h(y|x,\theta)}{h(y|x,\hat{\theta})})^{(\mathcal{T}-t)}] \leq 1$ using **Fact 1** and Eq. (8), we can establish $E_{(x,y) \sim (X,Y)}[g^{(\mathcal{T}-t)}(\theta)] \leq g(\theta)$. Let $\tilde{g}^{(\mathcal{T}-t)}(\theta) = E_{(x,y) \sim (X,Y)}[g^{(\mathcal{T}-t)}(\theta)]$ represents a fully adjusted prior across the entire sample space, akin to the true prior grounded on all available knowledge. Considering the non-negativity of the density function, we derive

$$\int \tilde{g}^{(\mathcal{T}-t)}(\theta) d\theta \leq 1. \quad (11)$$

Analogous to the interpretation of model misspecification, the updated prior distribution can be interpreted as assigning a non-negative probability mass to a pseudo model, while re-weighting the probability mass on models within the hypothesis space based on available data samples.

At this stage, our theory encompasses Bayesian inconsistency stemming from either model misspecification or improper priori, along with Bayesian posterior generalization for any \mathcal{T} value greater than 0.

3 Generalized Laplace Approximation

3.1 Laplace Approximation

Supervised deep learning operates within the framework of empirical risk minimization. Given an independent and identically distributed (i.i.d.) dataset $\mathcal{D} := \{(x_n, y_n)\}_{n=1}^N$ where $x_n \in \mathbb{R}^I$ represent inputs and $y_n \in \mathbb{R}^O$ denote outputs, a neural network $f(x, \theta) : \mathbb{R}^I \rightarrow \mathbb{R}^O$ with parameters $\theta \in \mathbb{R}^P$ is trained to minimize empirical risk. This involves minimizing a loss function expressed as the sum of empirical loss terms $\ell(x_n, y_n, \theta)$ and a regularizer $r(\theta)$

$$\begin{aligned} \theta_{\text{MAP}} &= \operatorname{argmin}_{\theta \in \mathbb{R}^P} \mathcal{L}(\mathcal{D}, \theta) \\ &= \operatorname{argmin}_{\theta \in \mathbb{R}^P} \left(\sum_{n=1}^N \ell(x_n, y_n, \theta) + r(\theta) \right). \end{aligned} \quad (12)$$

From a Bayesian perspective, these components correspond to i.i.d. log-likelihoods and a log-prior, respectively (Chen et al. [2024]), confirming that θ_{MAP} represents a maximum a posteriori (MAP) estimate:

$$\ell(x_n, y_n, \theta) = -\log p(y_n|x_n, \theta) \text{ and } r(\theta) = -\log p(\theta). \quad (13)$$

For instance, the commonly employed weight regularizer $r(\theta) = \frac{1}{2}\beta^{-2}\|\theta\|^2$ (also known as L2 regularizer) aligns with a Gaussian prior $p(\theta) = \mathcal{N}(0, \beta^2 I)$, while the cross-entropy loss represents a categorical likelihood. Therefore, the exponential of the negative training loss $\exp(-\mathcal{L}(\mathcal{D}, \theta))$ denotes an unnormalized posterior distribution. This can be demonstrated by substituting Eq. (13) into Eq. (1) and deriving

$$p(\theta|\mathcal{D}) = \frac{p(\mathcal{D}|\theta)p(\theta)}{\int_{\theta'} p(\mathcal{D}|\theta')p(\theta')d\theta'} = \frac{1}{Z} \exp(-\mathcal{L}(\mathcal{D}, \theta)), \quad (14)$$

where the evidence $Z = \int_{\theta'} p(\mathcal{D}|\theta')p(\theta')d\theta'$ denotes a constant normalization factor.

The Laplace approximation (MacKay [1991]) utilizes a second-order Taylor expansion of \mathcal{L} at the mode θ_{MAP} , resulting in an approximation:

$$\mathcal{L}(\mathcal{D}, \theta) \approx \mathcal{L}(\mathcal{D}, \theta_{\text{MAP}}) + \frac{1}{2}(\theta - \theta_{\text{MAP}})(\nabla_{\theta\theta}^2 \mathcal{L}(\mathcal{D}, \theta)|_{\theta=\theta_{\text{MAP}}})(\theta - \theta_{\text{MAP}})^T, \quad (15)$$

where the disappearance of the first-order Taylor expansion implies that θ_{MAP} corresponds to a minimum. Therefore, Z can be expressed as a Gaussian integral, for which the analytical solution is readily accessible (Daxberger et al. [2021]):

$$\begin{aligned} Z &= \int \exp(-\mathcal{L}(\mathcal{D}, \theta)) d\theta \\ &\approx \exp(-\mathcal{L}(\mathcal{D}, \theta_{\text{MAP}})) \int \exp(-\frac{1}{2}(\theta - \theta_{\text{MAP}})(\nabla_{\theta\theta}^2 \mathcal{L}(\mathcal{D}, \theta)|_{\theta=\theta_{\text{MAP}}})(\theta - \theta_{\text{MAP}})^T) d\theta \\ &= \exp(-\mathcal{L}(\mathcal{D}, \theta_{\text{MAP}}))(2\pi)^{\frac{P}{2}} (\det(\Sigma))^{\frac{1}{2}}. \end{aligned} \quad (16)$$

As a result, the posterior distribution is approximated with a multivariate Gaussian distribution, i.e., $p(\theta|\mathcal{D}) \approx \mathcal{N}(\theta_{\text{MAP}}, \Sigma)$. The covariance matrix Σ is determined by the Hessian of the posterior \mathcal{H} , indicated as $\Sigma = -[\mathcal{H}]^{-1}$ and $\mathcal{H} = \nabla_{\theta\theta}^2 \mathcal{L}(\mathcal{D}, \theta)|_{\theta=\theta_{\text{MAP}}}$.

Therefore, to obtain the approximate posterior using Laplace approximation, it is crucial to ascertain θ_{MAP} via conventional deep learning with a proper regularizer. The only additional step involves calculating the inverse of the Hessian matrix \mathcal{L} at θ_{MAP} . For the log-prior regularizer $r(\theta)$ in \mathcal{L} , which is defined by a Gaussian prior, the Hessian is straightforward, i.e., $\beta^{-2}I$ (Ritter et al. [2018]). Therefore,

$$\mathcal{H} = -NE_{(x,y) \sim \mathcal{D}}[\nabla_{\theta\theta}^2 \log p(y|x, \theta)|_{\theta=\theta_{\text{MAP}}}] - \beta^{-2}I. \quad (17)$$

3.2 Generalized Laplace Approximation

Here, we introduce the temperature parameter \mathcal{T} to generalize the posterior distribution and obtain:

$$p_{\mathcal{T}}(\theta|\mathcal{D}) = \frac{p(\mathcal{D}|\theta)^{\mathcal{T}} p(\theta)}{\int_{\theta'} p(\mathcal{D}|\theta')^{\mathcal{T}} p(\theta') d\theta'} = \frac{1}{Z_{\mathcal{T}}} \exp(-\mathcal{L}_{\mathcal{T}}(\mathcal{D}, \theta)), \quad (18)$$

$$\mathcal{L}_{\mathcal{T}}(\mathcal{D}, \theta) = \mathcal{T} \sum_{n=1}^N \ell(x_n, y_n, \theta) + r(\theta), \quad (19)$$

$$Z_{\mathcal{T}} = \int_{\theta'} p(\mathcal{D}|\theta')^{\mathcal{T}} p(\theta') d\theta' = \int_{\theta'} \exp(-\mathcal{L}_{\mathcal{T}}(\mathcal{D}, \theta')) d\theta'. \quad (20)$$

This method allows us to derive a generalized loss function and normalization factor. By following a similar derivation as Eq. (16), we can once again analytically ascertain the value of $Z_{\mathcal{T}}$, which remains constant upon determining θ_{MAP} .

In (Wenzel et al. [2020]), Appendix M, it is demonstrated that in the standard Bayesian framework, the generalized normalizing constant $Z_{\mathcal{T}}$ varies with θ . However, we have shown that within the Laplace approximation, $Z_{\mathcal{T}}$ remains constant. This is because Laplace approximation is typically applied post-training of a neural network, resulting in the determination of θ_{MAP} . This characteristic allows for generalization by straightforwardly adjusting the computation of the Hessian matrix with a temperature factor.

Given that \mathcal{T} is constant, the Hessian matrix $\mathcal{H}_{\mathcal{T}}$ of $\mathcal{L}_{\mathcal{T}}(\mathcal{D}, \theta)$ is evident:

$$\mathcal{H}_{\mathcal{T}} = -\mathcal{T}NE_{(x,y) \sim \mathcal{D}}[\nabla_{\theta\theta}^2 \log p(y|x, \theta)|_{\theta=\theta_{\text{MAP}}}] - \beta^{-2}I. \quad (21)$$

For uncertainty estimation at a test point x^* , it is conventional to employ Monte Carlo integration to approximate the intractable expression $p(y|x^*, \mathcal{D}) = \int p(y|x^*, \theta)p(\theta|\mathcal{D})d\theta$. This entails generating S_{mc} samples $(\theta_s)_{s=1}^{S_{mc}}$ from the posterior distribution of network parameters, followed by Bayesian analysis, as described in the subsequent equations:

$$\begin{aligned} p(y|x^*, \mathcal{D}) &\approx \frac{1}{S_{mc}} \sum_{t=1}^{S_{mc}} p(y|x^*, \theta_s), \\ \theta_s &\sim \mathcal{N}(\theta_{\text{MAP}}, -[\mathcal{H}_{\mathcal{T}}]^{-1}). \end{aligned} \quad (22)$$

Because computing or inverting the Hessian matrix is often impractical, the positive semi-definite approximations of the Hessian matrix, including Fisher information matrix and generalized Gauss-Newton, are commonly employed (Immer et al. [2021]). Additionally, dimensionality reduction

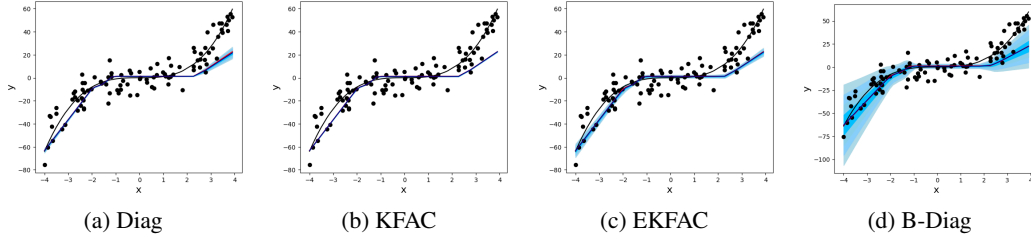


Figure 2: Uncertainty visualization for a toy regression dataset under $\mathcal{T} = 1$. Black dots represent data points, and a noiseless cubic function is shown by the black line. The red line indicates the deterministic prediction, while the blue line represents the mean of the predictive distribution. Additional standard deviations are depicted by various shades of blue.

techniques like Kronecker factorization (Ritter et al. [2018]) and low-rank approximation (Lee et al. [2020]) can be utilized. In Chen et al. [2024], it is noted that approximating the Hessian matrix can limit the spread of uncertainty. This effect on the value of \mathcal{T} will be examined in Section 4.

4 Experiments

4.1 Uncertainty Concentration Induced by Approximation

First, we visualize uncertainties arising from various Hessian approximations including diagonal approximation (Diag), Kronecker-factored approximate curvature (KFAC) (Ritter et al. [2018]), eigenvalue-corrected Kronecker factorization (EKFAC) (George et al. [2018]), block-diagonal approximation (B-Diag) (Martens and Grosse [2015]), on a toy regression dataset, similar to (Ritter et al. [2018], Hernández-Lobato and Adams [2015]). For detailed explanations of the Hessian approximations used in this experiment, please refer to Appendix A.1. We generate a dataset with 100 uniformly distributed points, $x \sim U(-4, 4)$, corresponding targets $y = x^3 + \epsilon$, where $\epsilon \sim N(0, 9)$. A two-layer neural network with seven units per layer is then used for model fitting. Fig. 2 illustrates the uncertainty of the same neural network resulting from diagonal, Kronecker-factored, eigenvalue-corrected Kronecker-factored, and block-diagonal Laplace methods. Note that the EKFAC method approximates the Hessian matrix with higher precision compared to KFAC, as detailed in George et al. [2018], Appendix A. Additionally, B-Diag offers the highest approximation precision among the mentioned methods, as it only isolates each layer within the neural network, assuming no correlation between weights across layers, a fundamental assumption of the other methods. Meanwhile, the estimated uncertainty generally follows the order: $\text{KFAC} < \text{Diag} < \text{EKFAC} < \text{B-Diag}$. We can have a preliminary hypothesis that the approximation of Hessian matrix can lead to the concentration of uncertainty, with finer approximations resulting in greater uncertainty. We will not examine this hypothesis in this paper, but we will evaluate how this effect influences the performance of the generalized Laplace approximation in the following section.

4.2 In-Distribution Experiments

Next, we analyze the performance of the generalized Laplace approximation under varying \mathcal{T} values and different Hessian approximations. We exclude B-Diag from this analysis, because even though B-Diag considers the covariance matrix of only one layer, in modern neural networks, its size remains large, being quadratic to the number of parameters in the layer. In this experiment, we use LeNet-5 (LeCun et al. [1998]) with ReLU activation and L2 regularization to fit the MNIST dataset, and ResNet-18 (He et al. [2016]) for the CIFAR-10 dataset (Krizhevsky et al. [2009]). The detailed architecture is provided in Appendix A.2. Notably, a fine-tuned pre-trained model is used to align more closely with the previously discussed theory, i.e., the pre-trained model can be regarded as θ_{MAP} .

Fig. 3 and 4 depict the performance, measured by accuracy and entropy, of the generalized Laplace approximation under varying \mathcal{T} values and different Hessian approximations. It is observed that both accuracy and entropy improve as \mathcal{T} increases for all three Hessian approximations. Specifically, the accuracy and entropy of Diag and EKFAC generally increase with \mathcal{T} and converge at $\mathcal{T} > 1$,

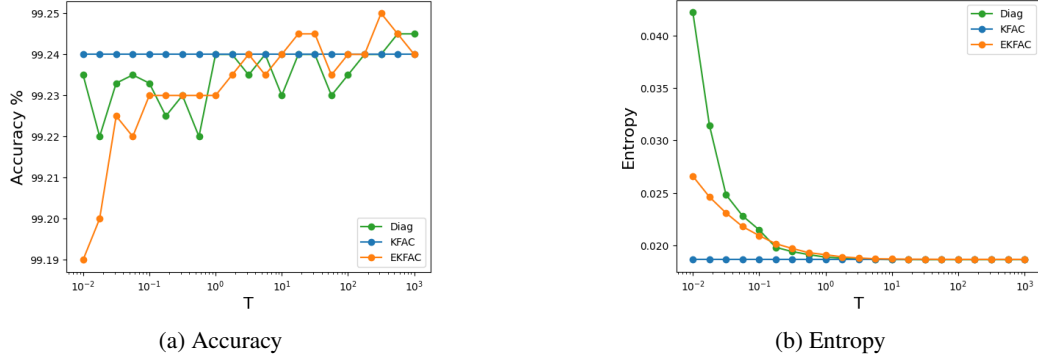


Figure 3: Predictive performance for a generalized LeNet-5 model on MNIST dataset. Note that the results for both in-distribution and out-of-distribution experiments are derived using Bayesian model averaging with a sample size of 50.

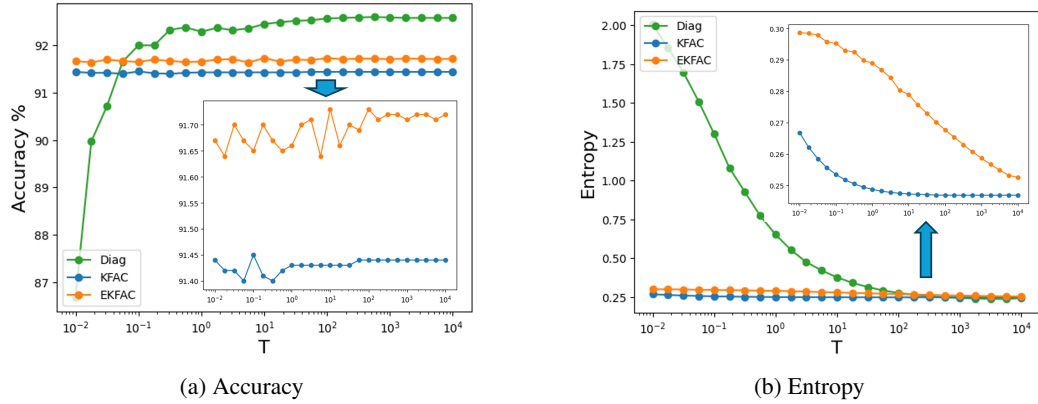
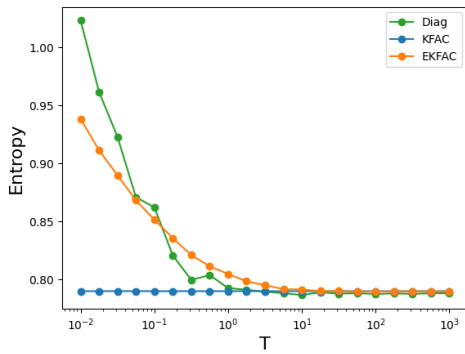


Figure 4: Predictive performance for a generalized ResNet-18 model on CIFAR-10 dataset. The curves of KFAC and EKfAC are magnified.

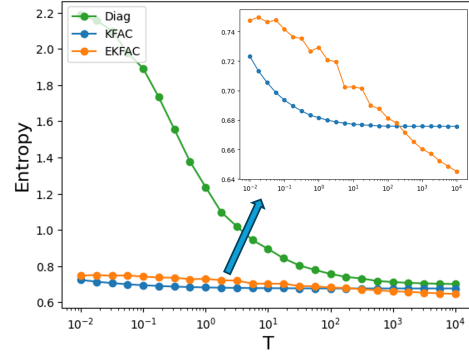
consistent with the findings in Wenzel et al. [2020]. Meanwhile, KFAC converges at \mathcal{T} slightly greater than 1 in Fig. 4 and at $\mathcal{T} < 1$ in Fig. 3. We attribute this to KFAC’s approximation, which results in extremely large Hessian matrix values (e.g., in the LeNet-5 experiment, the Frobenius norm of the Hessian matrix of the last layer is 1.0985×10^9 , significantly larger than that of Diag and EKfAC). The extremely large Hessian matrix values result in two outcomes: 1) the impact of \mathcal{T} is diminished, due to the huge difference in magnitude between the Hessian of the likelihood and the prior, and 2) the variance of the posterior distribution is down-scaled, causing the uncertainty concentration phenomenon discussed in Section 4.1. The issue with KFAC can arise from its computation using the Kronecker product of two matrices derived from input and backpropagation gradient, as detailed in Appendix A.1, whereas Diag’s computation relies solely on the gradient, and EKfAC involves a re-scaling.

4.3 Out-of-Distribution Experiments

In Section 4.2, we demonstrate that generalized Bayes can enhance the performance of Laplace approximation with an appropriately chosen \mathcal{T} . However, the optimal choice of \mathcal{T} is significantly influenced by the selected Hessian approximation. In this section, we extend our investigation of generalized Laplace approximation to out-of-distribution data. This aspect has been underexplored in existing research on generalized Bayes, due to the common assumption that Bayesian deep learning is inherently well-suited for such tasks based on its epistemic uncertainty estimation capacity.



(a) Entropy of a generalized LeNet-5 model trained on MNIST evaluated on Kuzushiji-MNIST dataset.



(b) Entropy of a generalized ResNet-18 model trained on CIFAR-10 evaluated on SVHN dataset.

Figure 5: Uncertainty estimation of generalized Laplace approximation on out-of-distribution datasets.

In this study, we use the Laplace approximation models trained in Section 4.2 to evaluate out-of-distribution datasets. Specifically, we assess LeNet-5 trained on the MNIST dataset using the Kuzushiji-MNIST test set (Clanuwat et al. [2018]) and ResNet-18 trained on CIFAR-10 using the SVHN test set (Netzer et al. [2011]). However, in contrast to in-distribution experiments, where we expect lower entropy, reflecting higher confidence in predictions on familiar data, in out-of-distribution, higher entropy is expected, indicating that the classifier produces more uniform predictions across its classes on unfamiliar data.

Fig. 5 presents the predictive uncertainties of generalized Laplace approximation models on out-of-distribution datasets. The generalized Laplace approximation demonstrates behavior consistent with in-distribution experiments. However, since high entropy is expected to yield uniform predictions, a small \mathcal{T} is preferred for out-of-distribution data, despite the scenario remains Bayesian deep learning. This can be attributed to the susceptibility of Bayesian deep learning to out-of-distribution data. D’Angelo and Henning [2021] propose that there exists a fundamental conflict between achieving strong generalization performance by integrating priors with high uncertainty when dealing with out-of-distribution data. According to Izmailov et al. [2021], Appendix G, it is found that the temperature factor can enhance performance on out-of-distribution data arising from Gaussian noise corruption, but does not notably improve performance in cases of other types of test data corruption (note that the out-of-distribution data in this experiment is caused by domain shift).

5 Conclusion

In this study, we introduce a cohesive theoretical framework for understanding how the generalized posterior addresses model misspecification in statistical Bayesian learning and inadequate priors in Bayesian deep learning. Additionally, we propose a method called generalized Laplace approximation, which integrates the concept of generalized Bayes into Laplace approximation. This method can improve performance on in-distribution data with an appropriately chosen \mathcal{T} , although the optimal \mathcal{T} selection is notably impacted by the chosen Hessian approximation. Furthermore, we empirically demonstrate the vulnerability of the generalized Laplace approximation to out-of-distribution data induced by domain shift.

An evident expansion of this research is to explore new strategies to address the susceptibility of the generalized Laplace approximation of out-of-distribution data. For example, integrating an appropriate prior could offer a solution to this issue, such as a Gaussian process prior with a radial basis function kernel to disregard prior knowledge, or employing the data empirical covariance prior (Izmailov et al. [2021]) to prevent the posterior from aligning with the prior along corresponding parameter space directions.

References

- Laurence Aitchison. A statistical theory of cold posteriors in deep neural networks. *arXiv preprint arXiv:2008.05912*, 2020.
- Zeyuan Allen-Zhu, Yuanzhi Li, and Yingyu Liang. Learning and generalization in overparameterized neural networks, going beyond two layers. *Advances in neural information processing systems*, 32, 2019.
- Andrew R Barron and Thomas M Cover. Minimum complexity density estimation. *IEEE transactions on information theory*, 37(4):1034–1054, 1991.
- Peter L Bartlett, Olivier Bousquet, and Shahar Mendelson. Local rademacher complexities. 2005.
- Pier Giovanni Bissiri, Chris C Holmes, and Stephen G Walker. A general framework for updating belief distributions. *Journal of the Royal Statistical Society Series B: Statistical Methodology*, 78(5):1103–1130, 2016.
- David M Blei, Alp Kucukelbir, and Jon D McAuliffe. Variational inference: A review for statisticians. *Journal of the American statistical Association*, 112(518):859–877, 2017.
- Yinsong Chen, Samson Yu, Jason K Eshraghian, and Chee Peng Lim. Sparse subnetwork inference for neural network epistemic uncertainty estimation with improved hessian approximation. *APL Machine Learning*, 2(2), 2024.
- Tarin Clanuwat, Mikel Bober-Irizar, Asanobu Kitamoto, Alex Lamb, Kazuaki Yamamoto, and David Ha. Deep learning for classical japanese literature. *arXiv preprint arXiv:1812.01718*, 2018.
- Francesco D’Angelo and Christian Henning. Uncertainty-based out-of-distribution detection requires suitable function space priors. 2021.
- Erik Daxberger, Agustinus Kristiadi, Alexander Immer, Runa Eschenhagen, Matthias Bauer, and Philipp Hennig. Laplace redux-effortless bayesian deep learning. *Advances in Neural Information Processing Systems*, 34:20089–20103, 2021.
- Simon S Du, Xiyu Zhai, Barnabas Poczos, and Aarti Singh. Gradient descent provably optimizes over-parameterized neural networks. *arXiv preprint arXiv:1810.02054*, 2018.
- Tim Erven, Steven Rooij, and Peter Grünwald. Catching up faster in bayesian model selection and model averaging. *Advances in Neural Information Processing Systems*, 20, 2007.
- Thomas George, César Laurent, Xavier Bouthillier, Nicolas Ballas, and Pascal Vincent. Fast approximate natural gradient descent in a kronecker factored eigenbasis. *Advances in Neural Information Processing Systems*, 31, 2018.
- Peter Grünwald. The safe bayesian: learning the learning rate via the mixability gap. In *International Conference on Algorithmic Learning Theory*, pages 169–183. Springer, 2012.
- Peter Grünwald and John Langford. Suboptimal behavior of bayes and mdl in classification under misspecification. *Machine Learning*, 66:119–149, 2007.
- Peter Grünwald and Thijs van Ommen. Inconsistency of bayesian inference for misspecified linear models, and a proposal for repairing it. *Bayesian Analysis*, 12(4):1069–1103, 2017.
- Peter D Grünwald and Nishant A Mehta. Fast rates for general unbounded loss functions: from erm to generalized bayes. *Journal of Machine Learning Research*, 21(56):1–80, 2020.
- Chuan Guo, Geoff Pleiss, Yu Sun, and Kilian Q Weinberger. On calibration of modern neural networks. In *International conference on machine learning*, pages 1321–1330. PMLR, 2017.
- Kaiming He, Xiangyu Zhang, Shaoqing Ren, and Jian Sun. Deep residual learning for image recognition. In *Proceedings of the IEEE conference on computer vision and pattern recognition*, pages 770–778, 2016.
- Jonathan Heek and Nal Kalchbrenner. Bayesian inference for large scale image classification. *arXiv preprint arXiv:1908.03491*, 2019.

- Rianne Heide, Alisa Kirichenko, Peter Grunwald, and Nishant Mehta. Safe-bayesian generalized linear regression. In *International Conference on Artificial Intelligence and Statistics*, pages 2623–2633. PMLR, 2020.
- José Miguel Hernández-Lobato and Ryan Adams. Probabilistic backpropagation for scalable learning of bayesian neural networks. In *International conference on machine learning*, pages 1861–1869. PMLR, 2015.
- Chris C Holmes and Stephen G Walker. Assigning a value to a power likelihood in a general bayesian model. *Biometrika*, 104(2):497–503, 2017.
- Alexander Immer, Maciej Korzepa, and Matthias Bauer. Improving predictions of bayesian neural nets via local linearization. In *International conference on artificial intelligence and statistics*, pages 703–711. PMLR, 2021.
- Pavel Izmailov, Patrick Nicholson, Sanae Lotfi, and Andrew G Wilson. Dangers of bayesian model averaging under covariate shift. *Advances in Neural Information Processing Systems*, 34:3309–3322, 2021.
- Laurent Valentin Jospin, Hamid Laga, Farid Boussaid, Wray Buntine, and Mohammed Bennamoun. Hands-on bayesian neural networks—a tutorial for deep learning users. *IEEE Computational Intelligence Magazine*, 17(2):29–48, 2022.
- Alex Krizhevsky, Geoffrey Hinton, et al. Learning multiple layers of features from tiny images. 2009.
- Yann LeCun, Léon Bottou, Yoshua Bengio, and Patrick Haffner. Gradient-based learning applied to document recognition. *Proceedings of the IEEE*, 86(11):2278–2324, 1998.
- Jongseok Lee, Matthias Humt, Jianxiang Feng, and Rudolph Triebel. Estimating model uncertainty of neural networks in sparse information form. In *International Conference on Machine Learning*, pages 5702–5713. PMLR, 2020.
- Benedict Leimkuhler, Charles Matthews, and Tiffany Vlaar. Partitioned integrators for thermodynamic parameterization of neural networks. *Foundations of Data Science*, 1(4):457–489, 2019.
- Yuanzhi Li and Yingyu Liang. Learning overparameterized neural networks via stochastic gradient descent on structured data. *Advances in neural information processing systems*, 31, 2018.
- David MacKay. Bayesian model comparison and backprop nets. *Advances in neural information processing systems*, 4, 1991.
- James Martens and Roger Grosse. Optimizing neural networks with kronecker-factored approximate curvature. In *International conference on machine learning*, pages 2408–2417. PMLR, 2015.
- Ulrich K Müller. Risk of bayesian inference in misspecified models, and the sandwich covariance matrix. *Econometrica*, 81(5):1805–1849, 2013.
- Radford M Neal et al. Mcmc using hamiltonian dynamics. *Handbook of markov chain monte carlo*, 2(11):2, 2011.
- Yuval Netzer, Tao Wang, Adam Coates, Alessandro Bissacco, Baolin Wu, Andrew Y Ng, et al. Reading digits in natural images with unsupervised feature learning. In *NIPS workshop on deep learning and unsupervised feature learning*, volume 2011, page 7. Granada, Spain, 2011.
- Kazuki Osawa, Siddharth Swaroop, Mohammad Emtiyaz E Khan, Anirudh Jain, Runa Eschenhagen, Richard E Turner, and Rio Yokota. Practical deep learning with bayesian principles. *Advances in neural information processing systems*, 32, 2019.
- Hippolyt Ritter, Aleksandar Botev, and David Barber. A scalable laplace approximation for neural networks. In *6th International Conference on Learning Representations, ICLR 2018-Conference Track Proceedings*, volume 6. International Conference on Representation Learning, 2018.
- Nicholas Syring and Ryan Martin. Calibrating general posterior credible regions. *Biometrika*, 106(2): 479–486, 2019.

- Tim Van Erven, Peter D Grünwald, Nishant A Mehta, Mark D Reid, and Robert C Williamson. Fast rates in statistical and online learning. *The Journal of Machine Learning Research*, 16(1): 1793–1861, 2015.
- Vladimir Vapnik. *The nature of statistical learning theory*. Springer science & business media, 2013.
- Stephen Walker and Nils Lid Hjort. On bayesian consistency. *Journal of the Royal Statistical Society Series B: Statistical Methodology*, 63(4):811–821, 2001.
- Florian Wenzel, Kevin Roth, Bastiaan S Veeling, Jakub Świątkowski, Linh Tran, Stephan Mandt, Jasper Snoek, Tim Salimans, Rodolphe Jenatton, and Sebastian Nowozin. How good is the bayes posterior in deep neural networks really? In *Proceedings of the 37th International Conference on Machine Learning*, pages 10248–10259, 2020.
- Yuling Yao, Aki Vehtari, Daniel Simpson, and Andrew Gelman. Using stacking to average bayesian predictive distributions (with discussion). *Bayesian Analysis*, 13(3), 2018.
- Guodong Zhang, Shengyang Sun, David Duvenaud, and Roger Grosse. Noisy natural gradient as variational inference. In *International conference on machine learning*, pages 5852–5861. PMLR, 2018.
- Ruqi Zhang, Chunyuan Li, Jianyi Zhang, Changyou Chen, and Andrew Gordon Wilson. Cyclical stochastic gradient mcmc for bayesian deep learning. In *8th International Conference on Learning Representations, ICLR 2020*, 2020.
- Tong Zhang. From ε -entropy to kl-entropy: Analysis of minimum information complexity density estimation. *The Annals of Statistics*, pages 2180–2210, 2006.

A Appendix

A.1 Hessian Approximations

One positive semi-definite approximation to estimate $E_{(x,y) \sim \mathcal{D}}[\nabla_{\theta\theta}^2 \log p(y|x, \theta)|_{\theta=\theta_{\text{MAP}}}]$ in modern automatic differentiation frameworks is the Fisher information matrix (FIM), which is simply the expectation of the squared gradients:

$$FIM = E_{(x,y) \sim \mathcal{D}}[(\nabla_{\theta} \log p(y|x, \theta))]. \quad (23)$$

The matrix FIM has dimensions of $\#\theta \times \#\theta$, making it computationally impractical to calculate and invert. Consequently, it is often subject to further approximation. A common simplification, adopted by previous methods, involves treating each layer in the neural network independently, assuming no correlation between weights across layers. This results in an initial block-diagonal approximation of the FIM, with each block FIM_l corresponding to the parameters of a specific layer l . Nevertheless, in deep neural networks, FIM_l can still be considerably large.

A cost-effective yet basic approach employs a diagonal FIM_l to address variance in individual parameter dimensions, ignoring the covariance structure. To incorporate parameter covariance, KFAC provides a more comprehensive alternative. KFAC decomposes each FIM_l into a Kronecker product of two smaller matrices, substantially decreasing storage, computation, and inversion expenses:

$$FIM_l \approx Q \otimes G. \quad (24)$$

In layer l , the input $q \in \mathbb{R}^{I_l}$ is processed to calculate the backpropagated gradient $g \in \mathbb{R}^{O_l}$ of the linear pre-activations, i.e., $a = W^T q$. The bias terms are included in W by attaching a 1 to every q . The gradients with respect to the parameters $\theta_l = W$ are written as $\nabla_{\theta_l} = \frac{\partial \ell}{\partial \theta_l} = qg^T$. Given that the FIM can be expressed as the expectation of squared gradients, i.e., $FIM_l = E[\nabla_{\theta_l} \nabla_{\theta_l}^T]$, the Kronecker-factored approximation of FIM_l utilizes the matrices $Q = E[qq^T] \in \mathbb{R}^{I_l \times I_l}$ and $G_n = E[gg^T] \in \mathbb{R}^{O_l \times O_l}$. The KFAC can be derived in the following manner:

$$FIM_l = E[\nabla_{\theta_l} \nabla_{\theta_l}^T] = E[(qg^T)(qg^T)^T] \approx E[qq^T]E[gg^T]. \quad (25)$$

Table 1: The architecture of LeNet-5.

layer	details
convolution_1	kernel 5×5 , channel 6, padding 2
max_pooling_1	kernel 2×2 , stride 2
convolution_2	kernel 5×5 , channel 16
maxpooling_2	kernel 2×2 , stride 2
fully_connected_1	output shape 120
fully_connected_2	output shape 84
fully_connected_3	output shape 10

Table 2: The architecture of ResNet-18.

layer	details			
convolution_1	kernel 7×7 , channel 64, stride 2			
max_pooling	kernel 3×3 , stride 2			
block_1	<table border="1" style="display: inline-table; vertical-align: middle;"> <tr> <td>convolution_11(kernel 3×3, channel 64, stride 2)</td> <td rowspan="2" style="vertical-align: middle;">$\times 2$</td> </tr> <tr> <td>convolution_12(kernel 3×3, channel 64)</td> </tr> </table>	convolution_11(kernel 3×3 , channel 64, stride 2)	$\times 2$	convolution_12(kernel 3×3 , channel 64)
convolution_11(kernel 3×3 , channel 64, stride 2)	$\times 2$			
convolution_12(kernel 3×3 , channel 64)				
block_2	<table border="1" style="display: inline-table; vertical-align: middle;"> <tr> <td>convolution_21(kernel 3×3, channel 128, stride 2)</td> <td rowspan="2" style="vertical-align: middle;">$\times 2$</td> </tr> <tr> <td>convolution_22(kernel 3×3, channel 128)</td> </tr> </table>	convolution_21(kernel 3×3 , channel 128, stride 2)	$\times 2$	convolution_22(kernel 3×3 , channel 128)
convolution_21(kernel 3×3 , channel 128, stride 2)	$\times 2$			
convolution_22(kernel 3×3 , channel 128)				
block_3	<table border="1" style="display: inline-table; vertical-align: middle;"> <tr> <td>convolution_31(kernel 3×3, channel 256, stride 2)</td> <td rowspan="2" style="vertical-align: middle;">$\times 2$</td> </tr> <tr> <td>convolution_32(kernel 3×3, channel 256)</td> </tr> </table>	convolution_31(kernel 3×3 , channel 256, stride 2)	$\times 2$	convolution_32(kernel 3×3 , channel 256)
convolution_31(kernel 3×3 , channel 256, stride 2)	$\times 2$			
convolution_32(kernel 3×3 , channel 256)				
block_4	<table border="1" style="display: inline-table; vertical-align: middle;"> <tr> <td>convolution_41(kernel 3×3, channel 512, stride 2)</td> <td rowspan="2" style="vertical-align: middle;">$\times 2$</td> </tr> <tr> <td>convolution_42(kernel 3×3, channel 512)</td> </tr> </table>	convolution_41(kernel 3×3 , channel 512, stride 2)	$\times 2$	convolution_42(kernel 3×3 , channel 512)
convolution_41(kernel 3×3 , channel 512, stride 2)	$\times 2$			
convolution_42(kernel 3×3 , channel 512)				
average_pooling	output shape $512 \times 1 \times 1$			
fully_connected	output shape 10			

Consider the eigendecomposition $FIM_l = USU^T$. By using the transformation $S = U^T FIM_l U = E[U^T \nabla_{\theta_l} \nabla_{\theta_l}^T U]$, we obtain $S_{ii} = E[(U^T \nabla_{\theta_l})_p^2]$ for $p \in 1, \dots, P_l$. When applying the Kronecker approximation, the eigendecomposition of the Kronecker product $Q \otimes G$ of two real symmetric positive semi-definite matrices Q and G can be written as $Q = U_Q S_Q U_Q^T$ and $G = U_G S_G U_G^T$, yielding $Q \otimes G = (U_Q \otimes U_G)(S_Q \otimes S_G)(U_Q \otimes U_G)^T$. Thus, enhancements to the Kronecker approximation can be attained by replacing $(S_Q \otimes S_G)pp$ with $S'_{ii} = E[((U_Q \otimes U_G)^T \nabla_{\theta})_p^2]$, leading to an improved approximation:

$$FIM'_l = (U_Q \otimes U_G)S'(U_Q \otimes U_G)^T. \quad (26)$$

The FIM'_l is known as EKFac, denoting the eigenvalue-corrected Kronecker product approximation of curvature.

A.2 Experiment Setup

This section provides the complete experimental details of the work described in the main paper.

The models used in the numerical experiments in this study include LeNet-5 and ResNet-18. LeNet-5 comprises two convolutional layers and three fully connected layers, with its detailed architecture provided in Table 1. ResNet-18 consists of a single convolutional layer, a max-pooling layer, four residual modules (each containing two residual blocks with two convolutional layers per block), an average-pooling layer, and a fully connected layer. The detailed architecture of ResNet-18 is shown in Table 2. Additionally, a weight decay of 0.01 is used during training, and the value of β^{-2} is adjusted to ensure the Hessian matrix approximation is positive-definite. Furthermore, data augmentation with a sample size of 30 is used to facilitate the calculation of Hessian approximations.

The training is conducted on MNIST and CIFAR-10 datasets, while the evaluation stage varies between in-distribution and out-of-distribution experiments. In-distribution experiments are performed on the MNIST and CIFAR-10 test datasets. Out-of-distribution experiments use the Kuzushiji-MNIST and SVHN test datasets to assess the predictive performance of the generalized Laplace approximation on different data distributions. Additionally, 50 samples of θ will be drawn from the posterior distribution to estimate uncertainty on the test dataset, in accordance with Eq. (22).